Computers and Mathematics with Applications 67 (2014) 437–444

Contents lists available at ScienceDirect

Computers and Mathematics with Applications

journal homepage: www.elsevier.com/locate/camwa

Mechanism of axis switching in low aspect-ratio rectangular jets

Nan Chen, Huidan Yu *

Department of Mechanical Engineering, Indiana University-Purdue University Indianapolis, IN 46202, USA

ARTICLE INFO

Keywords:
Rectangular jet
Axis-switching
Secondary flow
Lattice Boltzmann method

ABSTRACT

In this work we systematically study one square jet ($AR = 1$) and four rectangular jets with an aspect ratio of width over height $AR = 1.5$, 2, 2.5, and 3 respectively using the lattice Boltzmann method for direct numerical simulation. Focuses are on various flow properties on transverse planes downstream to investigate the correlation between the downstream velocity and secondary flow. Three distinct regions of jet development are identified in all the five jets. As the length of the PC (potential core) region maintains about the same, that of the CD (characteristic decay) region strongly depends on the jet aspect-ratio (AR) and Reynolds number (Re). The 45° and 90° axis-switching occur in the CD region, with the former followed by the latter at the early and late stages of the CD region respectively. The half-width streamwise velocity contour reveals that 45° axis-switching is mainly contributed by the corner effect, whereas the aspect-ratio (elliptic) feature affects the shape of the jet when 45° axis-switching occurs. The close examinations of flow pattern and vorticity contour, as well as the correlation between streamwise velocity and vorticity, indicate that 90° axis-switching results from the boundary effect. Specific flow patterns for 45° and 90° axis-switching are identified to reveal the mechanism of the axis-switchings respectively.

Published by Elsevier Ltd

1. Introduction

Noncircular jets attract special attentions due to their enhanced entrainment and mixing properties, relative to those of comparable axisymmetric jets (Ref. [1] and references therein). Depending on initial conditions at the jet inlet, the cross-section of noncircular jets can evolve downstream through shapes similar to that at the jet inlet with its major and minor axis rotated at angles depending on the jet geometry. This phenomenon is called axis-switching. In the last few decades, axis-switching has been observed in various noncircular jets, e.g. elliptic jets [2–12], rectangular jets [13–21], and other more complicated noncircular jets [22–24]. The jet dynamics is of great interest from both fundamental physics and practical application point of view. It has been believed that in elliptic jets, the underlying mechanism of axis-switching behavior results from self-induced Biot–Savart deformation of vortex rings due to nonuniform azimuthal curvature and interaction between azimuthal and streamwise vorticities [1]. Recently, an experiment confirmed the azimuthal vortex deformation in the region of the axis-switching of a lobed orifice jet [23]. Rectangular jets combine the variable aspect-ratio feature of elliptic jet with the corner vortex feature of square jets. The aspect-ratio (AR) is defined as the ratio of major to minor axis of the jet inlet. This combination yields features which do not appear in elliptic jets and are of importance in practical applications. One example is the 45° axis-switching in a square jet and both 45° and 90° axis-switchings in a rectangular jet ($AR = 1.5$) [20].

* Corresponding author.
E-mail addresses: whyu@iupui.edu, yuhd123@yahoo.com (H. Yu).

0898-1221/$ – see front matter. Published by Elsevier Ltd
http://dx.doi.org/10.1016/j.camwa.2013.03.018

The present study is a part of our continuous effort to investigate the mixing properties when a jet entrains with surroundings and enhance our capability to predict physics in turbulent rectangular jets. In our previous works [19], we performed large eddy simulations (LES) of turbulent rectangular jets at relatively high Reynolds numbers using the kinetic-based lattice Boltzmann method (LBM). The LBM has been well established as an alternative methodology of computational fluid dynamics for solving various complex flows [25,26]. It is second-order accurate in time and space and recovers Navier–Stokes equations in the incompressible limit [27]. The main physical and computational advantages of LBM include simplicity of programming, ease of handling complex geometry, suitability of massive parallel computing, etc.; thus, it is well suited for simulating complex flows including various jet flows [19,28,29]. In the previous study of turbulent rectangular jets [19], we obtained various turbulence statistics which agreed reasonably well with experimental data. Peculiar phenomena such as axis-switching and saddle-back velocity profile were observed. The former was well agreed with experimental observation but the latter was less profound than what observed in the experiment. However, the mechanism of them remained unrevealed due to the usage of a laminar velocity profile at the jet inlet, the complexity of turbulent mixing, and the demanding computation cost. We are inspired to study jet development in laminar rectangular jets to find out what causes axis-switching in laminar jets and what the mechanism behind is to gain insights about how to further explore mixing properties in turbulent jets.

In this study, we systematically study axis-switching in five low AR rectangular jets with $AR = 1, 1.5, 2, 2.5, 3$ at relatively low Reynolds numbers through direct numerical simulation (DNS) using LBM. Focus is on the correlations between the primary downstream penetrating flow and the secondary entertainment on transverse planes to reveal the mechanism of axis-switching in rectangular jets. The remainder of this paper is organized as follows. Section 2 introduces the lattice Boltzmann method for DNS of rectangular jets. In Section 3, we show results on the mechanism of 45° and 90° axis-switching through the correlations between the primary downstream velocity and the vorticity on transverse planes. We conclude in Section 4 with a short discussion.

2. Lattice Boltzmann method for rectangular jets

We employ a D3Q19 single-relaxation-time (SRT) lattice model for the simulation. In this lattice model, the 3D discrete phase space is defined by cubic lattice with 19 discrete particle velocities $\boldsymbol{e}_\alpha$ given as

$$\boldsymbol{e}_\alpha = \begin{cases} (0,0,0), & \alpha = 0 \\ (\pm 1,0,0),\ (0,\pm 1,0),\ (0,0,\pm 1), & \alpha = 1 \sim 6 \\ (\pm 1,\pm 1,0),\ (\pm 1,0,\pm 1),\ (0,\pm 1,\pm 1), & \alpha = 7 \sim 18. \end{cases} \tag{1}$$

The SRT lattice Boltzmann equation is expressed as

$$f_\alpha(\boldsymbol{r} + \boldsymbol{e}_\alpha \delta_t, t + \delta_t) = f_\alpha(\boldsymbol{r}, t) - \frac{1}{\tau}[f_\alpha(\boldsymbol{r}, t) - f_\alpha^{(eq)}(\boldsymbol{r}, t)] \tag{2}$$

where f_α and f_α^{eq} ($\alpha = 0, 1, \ldots, 18$) represent the 19 distribution functions and their equilibria, respectively; δ_t is the discrete time-step, and τ is the relaxation time. The equilibria for incompressible flow are [30]

$$f_\alpha^{(eq)} = \omega_\alpha \left\{ \delta\rho + \rho_0 \left[\frac{3\boldsymbol{e}_\alpha \cdot \boldsymbol{u}}{c^2} + \frac{9(\boldsymbol{e}_\alpha \cdot \boldsymbol{u})^2}{2c^4} - \frac{3u^2}{2c^2} \right] \right\} \tag{3}$$

where $\delta\rho$ is the density fluctuation, ρ_0 is the constant mean density of the system, and $c = \delta x/\delta t$. In LBM the values of ρ_0, δx, and δt are all typically set to unity. The sound speed in this model is $c_s = c/\sqrt{3}$. The total density is $\rho = \rho_0 + \delta\rho$. The weighting factors ω_α for the D3Q19 model are

$$\omega_\alpha = \begin{cases} \dfrac{1}{3}, & \alpha = 0 \\ \dfrac{1}{18}, & \alpha = 1 \sim 6 \\ \dfrac{1}{36}, & \alpha = 7 \sim 18. \end{cases} \tag{4}$$

The mass and momentum conservations are strictly enforced:

$$\delta\rho = \sum_\alpha f_\alpha = \sum_\alpha f_\alpha^{(eq)} \tag{5}$$

$$\rho_0 \boldsymbol{u} = \sum_\alpha \boldsymbol{e}_\alpha f_\alpha = \sum_\alpha \boldsymbol{e}_\alpha f_\alpha^{(eq)}. \tag{6}$$

The fluid kinematic viscosity ν has the following relation with the relaxation time τ:

$$\nu = \frac{1}{3}\left(\tau - \frac{1}{2}\right) c\delta_x, \quad \tau = \frac{3\nu}{c\delta_x} + \frac{1}{2} \tag{7}$$

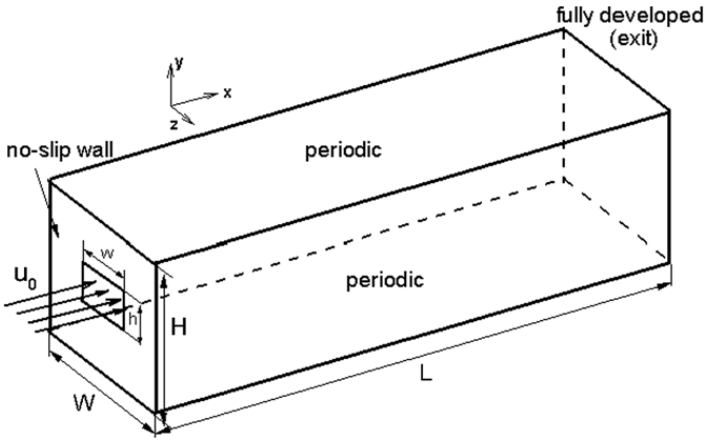

Fig. 1. Schematic of the computation set-up for a rectangular jet driven by a uniform velocity stream at the jet inlet ($x = 0$).

Table 1
Five jets conducted in this study. The unit for length is centimeter (cm).

Jet	*AR*	w, h	W, H, L	Jet grid size	Domain grid size
I	1	1.0, 1.0	6.3, 6.3, 100.0	8, 8	50, 50, 800
II	1.5	1.5, 1.0	6.3, 6.3, 100.0	12, 8	50, 50, 800
III	2	2.0, 1.0	6.3, 6.3, 100.0	16, 8	50, 50, 800
IV	2.5	2.5, 1.0	6.3, 6.3, 100.0	20,8	50, 50, 800
V	3	3.0, 1.0	6.3, 6.3, 126.0	24, 8	50, 50, 1000

3. Numerical results on axis-switching behavior and mechanism behind

The coordinate system of the simulation field is shown in Fig. 1. The x, y, and z axes are parallel to streamwise, lateral and spanwise directions respectively. The whole domain is a $W \times H \times L$ channel. The flow issues with a uniform velocity u_0 from a $w \times h$ orifice slot located at the center of the plane ($x = 0$, $-w/2 \le z \le w/2$, and $-h/2 \le y \le h/2$). The *Re* is based on the lateral dimension h of the jet inlet, jet inlet velocity, and kinematic viscosity $\nu = 1.51\text{e} - 5(m^2/s)$. The jet orifice is simplified as a plane where we apply for generalized bounce-back boundary [31]

$$f_\alpha^* = f_\alpha - 6\omega_\alpha \rho_0 \boldsymbol{u}_0 \cdot \boldsymbol{e}_\alpha \tag{8}$$

at jet orifice plane ($x = 0$) where f_α^* is the distribution function of $\boldsymbol{e}_\alpha^* = -\boldsymbol{e}_\alpha$, fully developed boundary at outflow ($x = L$), and periodic boundary conditions in both spanwise and lateral directions. In this work we study one square jet and four rectangular jets listed in Table 1 and focus on axis-switching phenomena and the mechanism behind.

Early experimental and analytical investigations [32–34] have revealed that fully developed flow field of a rectangular jet is characterized by three distinct regions: (i) PC (potential core) region into which the mixing initiated at the jet boundaries has not penetrated; (ii) CD (characteristic decay) region where velocity decay and mixing depend on the jet aspect ratio and shape; (iii) AD (axisymmetric decay) region extending to infinity where the velocity field is axisymmetric independent of the jet inlet shape. In this paper we focus on the near-field (PC and CD regions) jet features.

For the given dimension of the jets, we first identify the three characteristic regions for each jet at a representative Reynolds number (Re = 200) with $u_0 = 23.0$ (m/s) in Table 2 through monitoring the shape of jet through the half-width streamwise velocity contour (HWSVC) on each transverse planes at each downstream grid. The onset of the CD region is determined when the original lines and corners of the rectangular or square shape of the HWSVC become round, whereas the onset of the AC region is where the shape of the HWSVC becomes circular. It shows that the length of the PC region is independent of the jet *AR* when normalized by h, whereas the CD region varies with different *AR*s. The bigger the *AR*, the longer the length of the CD region. When *AR* changes from 1 to 3, the length of the CD region doubles. Meanwhile, the CD region has a strong dependence on the Re number. For a given jet, e.g. $AR = 2.5$, as shown in Table 3, the length of the CD region increases when Re increases.

We examine the shape of HWSVC to monitor axis-switching behavior. The HWSVC at a given downstream plane (x-plane) is the contour of the points $(y_{\text{hlf}}, z_{\text{hlf}})$ on the plane at which the streamwise velocity is one-half of the centerline streamwise velocity:

$$u(x, y_{\text{hlf}}, z_{\text{hlf}}) = \frac{1}{2}u(x, 0, 0). \tag{9}$$

The HWSVC is a direct measure of the level of jet mixing. Fast spreading of HWSVC indicates rapid entrainment and mixing. The physics of entrainment and HWSVC evolution can be understood by examining the secondary flow, i.e., flow on the transverse plane (y, z) normal to the primary flow direction (x). Fig. 2 shows the downstream evaluation of HWSVC at

Table 2
Lengths of PC, CD regions for different *AR*s at Re = 200.

Jet	*AR*	PC	CD	AD
I	1	$x \leq 0.4$ h	0.4 h $< x \leq$ 37.0 h	$x >$ 37.0 h
II	1.5	$x \leq 0.8$ h	0.8 h $< x \leq$ 57.0 h	$x >$ 57.0 h
III	2	$x \leq 0.8$ h	0.8 h $< x \leq$ 64.0 h	$x >$ 64.0 h
IV	2.5	$x \leq 0.8$ h	0.8 h $< x \leq$ 74.0 h	$x >$ 74.0 h
V	3	$x \leq 0.8$ h	0.8 h $< x \leq$ 82.0 h	$x >$ 82.0 h

Table 3
Lengths of PC, CD regions for different Res at *AR* = 2.5.

Re	PC	CD	AD
200	$x \leq 0.8$ h	0.8 h $< x \leq$ 74.0 h	$x >$ 74.0 h
254	$x \leq 0.8$ h	0.8 h $< x \leq$ 92.0 h	$x >$ 92.0 h
302	$x \leq 0.8$ h	0.8 h $< x \leq$ 105.0 h	$x >$ 105.0 h

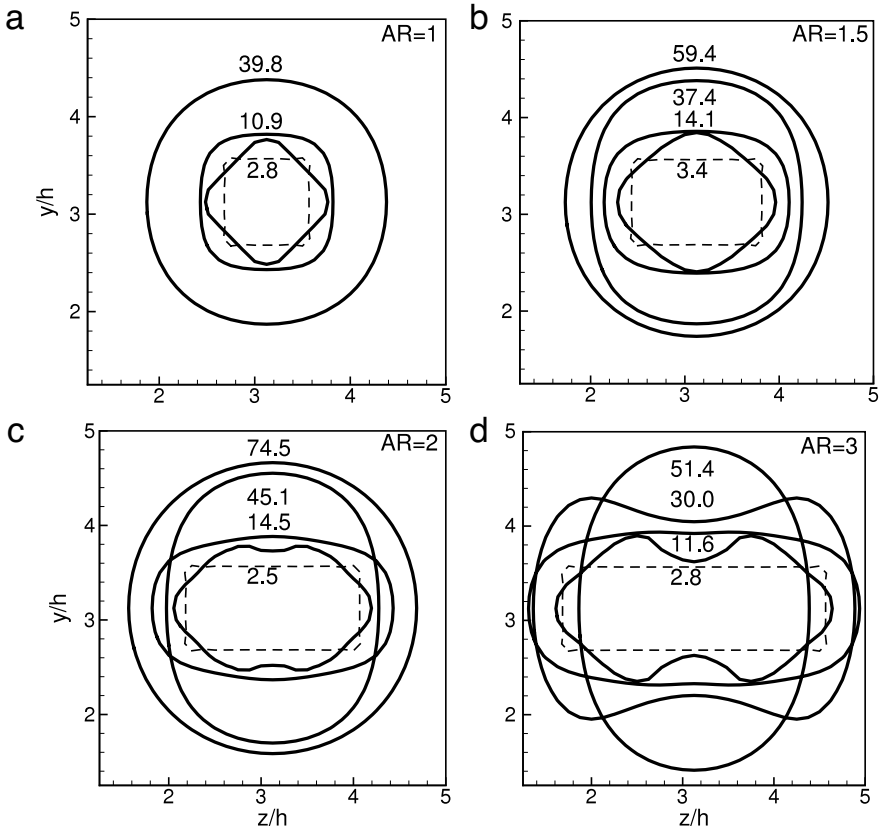

Fig. 2. HWSVC profiles on transverse planes of jet (a) I, (b) II, (c) III, (d) V at indicated representative downstream locations, Re = 200.

Re = 200 for jet (a) I, (b) II, (c) III, and (d) V at representative downstream locations. The numbers adjacent to the HWSVC lines in the figures are the downstream distance from the jet inlet normalized by the jet inlet height *h*. In the square jet (Fig. 2(a)), the jet starts from a square (dashed line) shape. The axes switch 45° at $x = 2.8$ h, and then switch back to a round square shape at $x = 10.9$ h. At location $x = 39.8$ h, the jet becomes axisymmetric, indicating that the AD region starts. As speculated, the AD region extends to infinity. The axis-switching in rectangular jets is more interesting since there will be two axis-switchings occurring downstream as shown in Fig. 2(b)–(c). For example, jet II ($AR = 1.5$) starts from a rectangular shape (dashed line) at the jet inlet, first switches 45° at $x = 3.4$ h, then switches back as a rounded rectangle at $x = 14.1$ h, then switches again to 90° at $x = 37.4$ h, and eventually becomes round at $x = 59.4$ h. The features of axis-switching in rectangular jets may be summarized as follows.

- 45° axis-switching occurs in all five rectangular jets at approximately the same downstream location independent of *AR*, implying that the 45° axis-switching results in the corner vortex feature unique in rectangular jets.
- The shape of jet when 45° axis-switching occurs varies from a diamond ($AR = 1$), to rhombus ($AR = 1.5$), to deformed rhombuses with saddle-back close to the center of the minor axis ($AR \geq 2$), indicating that the aspect ratio does affect

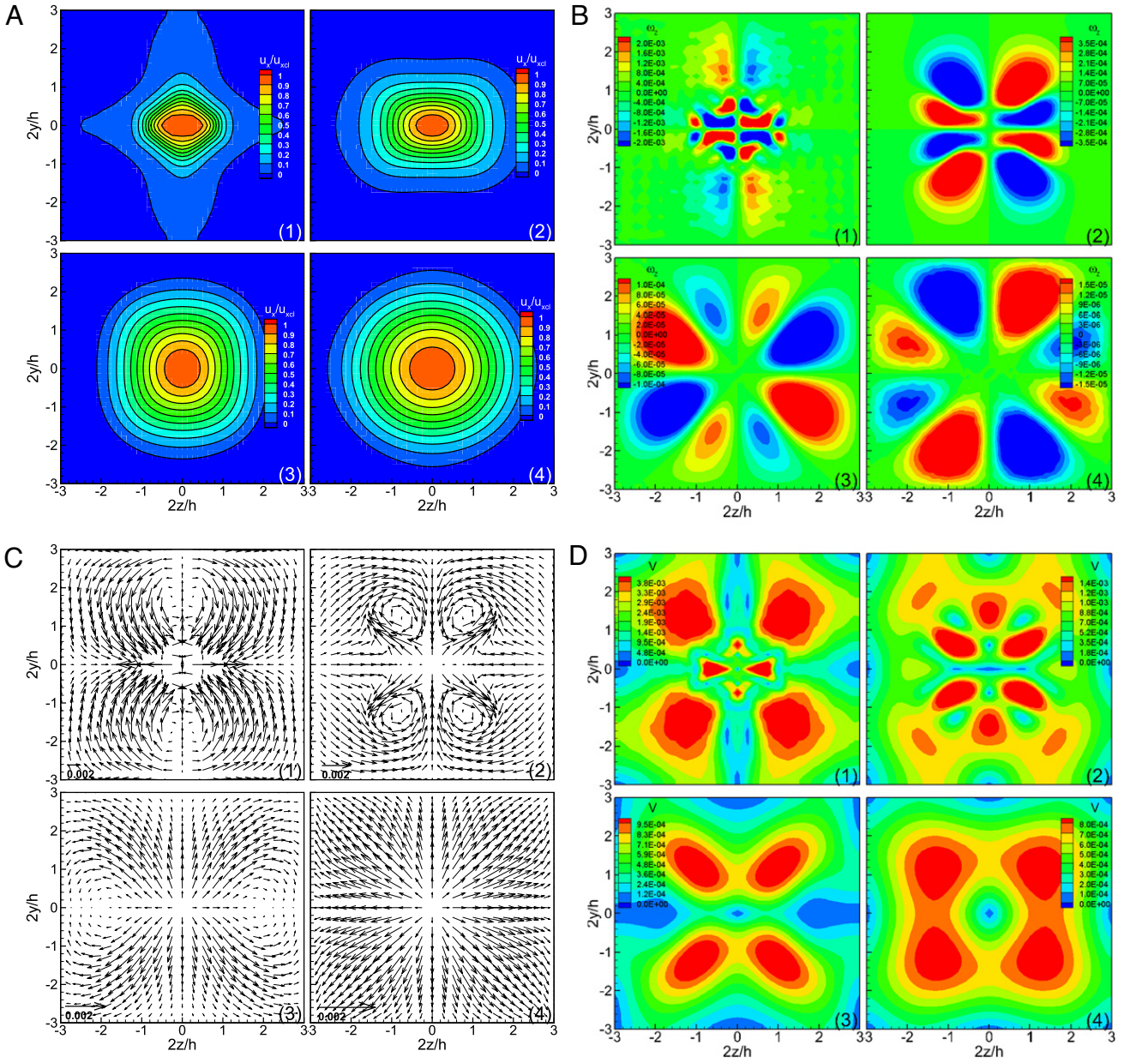

Fig. 3. Secondary flow properties of jet with $AR = 1.5$ on representative downstream planes: (1) $x = 3.4$ h; (2) $x = 14.1$ h; (3) $x = 37.4$ h; (4) $x = 59.4$ h, corresponding to the contour lines in Fig. 2(b). (A) contour fields of normalized penetrating velocity in the direction of jet propagates, u_x/u_{xcl}; (B) contour fields of vorticity $\omega_x = \frac{\partial u_z}{\partial y} - \frac{\partial u_y}{\partial z}$; (C) vector fields of the secondary flow, $\boldsymbol{V} = u_y\boldsymbol{j} + u_z\boldsymbol{k}$; (D) contour fields of velocity magnitude of the secondary flow, $V = \sqrt{u_y^2 + u_z^2}$.

the jet entrainment to the surrounding, which is a feature of elliptic jets. Thus, the axis-switchings in a rectangular jet are contributed by both corner effect and aspect-ratio effect.

- 90° axis-switching follows 45° axis-switching. A smaller *AR* jet develops the 90° axis-switching closer to the jet inlet than an larger *AR* jet.
- Both 45° and 90° happen in the CD region. The former is before the latter, implying that the corner feature is kicked in early then the elliptic feature.
- Saddle-back velocity profile observed in 45° axis-switching for relatively large *AR* jets is another peculiar behavior in rectangular jets reported in experiments [14,16,34–36] and computation [19], which will be a focus in our future study, thus not discussed here.

Close look has been taken on the correlation of penetrating velocity u_x of primary flow and secondary flow on transverse planes. Fig. 3 show various properties including normalized downstream velocity (u_x/u_{xcl}), downstream vorticity ($\omega_x = \frac{\partial u_z}{\partial y} - \frac{\partial u_y}{\partial z}$), secondary flow velocity ($\boldsymbol{V} = u_y\boldsymbol{j} + u_z\boldsymbol{k}$) and its magnitude ($V = \sqrt{u_y^2 + u_z^2}$) on representative downstream planes: (1) $x = 3.4$ h; (2) $x = 14.1$ h; (3) $x = 37.4$ h; (4) $x = 59.4$ h, corresponding to the contour lines in Fig. 2(b) for

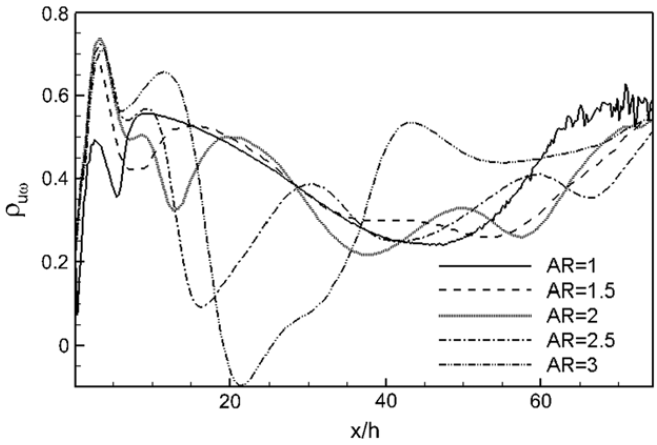

Fig. 4. Correlation functions of velocity and vorticity along downstream direction for the five jets. Solid line: $AR = 1$; dashed line: $AR = 1.5$; dotted line: $AR = 2$; dash-dot line: $AR = 2.5$; dash-dot-dot line: $AR = 3$.

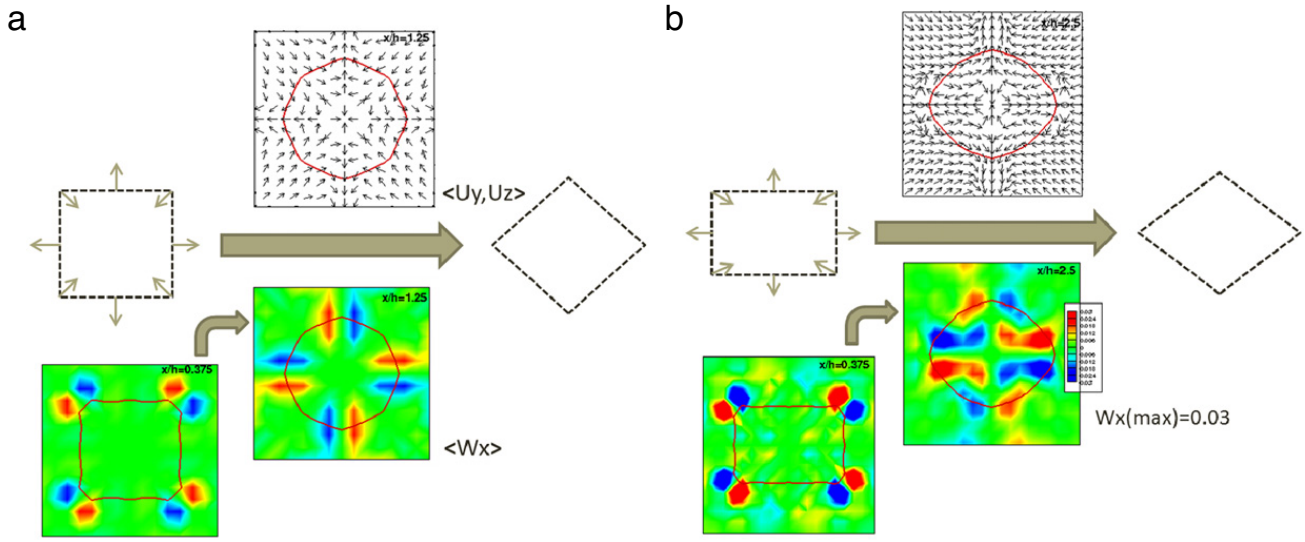

Fig. 5. Driven mechanism of flow and vorticity patterns for 45° axis-switching. (a) square jet ($AR = 1$); (b) rectangular jet ($AR = 1.5$).

jet II ($AR = 1.5$). The four representative downstream planes correspond to the typical stages of the jet development, 45° axis-switching, round rectangle, 90°, and circle as described above where only the half-velocity contour ($u_x/u_{xcl} = 0.5$) lines showed. From Fig. 3(A), it is seen that axis-switchings, both 45° and 90°, occur on almost all the levels of u_x/u_{xcl}. The 45° axis-switching (Fig. 3(A) (1)) seems more significant when the velocity ratio reduces outward, whereas the 90° axis-switching (Fig. 3(A) (3)) is stronger when the velocity ratio is large. The corresponding vorticity contours, secondary vector fields and their magnitude contours are shown in Fig. 3(B)–(D). We will discuss these patterns later.

Inspired by the fact that the secondary flow is induced due to the entrainment with the surroundings when the jet is penetrating downstream, we define the correlation function of penetrating velocity u_x and vorticity ω_x as

$$\rho_{u\omega} = \frac{cov(u_x, |\omega_x|)}{\sigma_{u_x}\sigma_{|\omega_x|}} = \frac{\langle (u_x(m,n) - \langle u_x\rangle)\,(\omega_x(m,n) - \langle|\omega_x|\rangle)\rangle}{\sqrt{\langle (u_x(m,n) - \langle u_x\rangle)^2\rangle \langle (|\omega_x(m,n)| - \langle|\omega_x|\rangle)^2\rangle}} \tag{10}$$

where $\langle\cdots\rangle$ represents volume averaging for homogeneous turbulence and where summation over repeated indices is understood. Fig. 4 shows the correlation functions of velocity and vorticity along downstream direction for the five jets. It is shown that velocity and vorticity quickly team up to a peak after the jet starts to develop. Close examination indicates that the 45° axis-switching occurs right after the peak in each jet. In the course to develop 90° axis-switching, the correlation function fluctuates quite a bit, shifting between coloration and decoloration, and bigger AR jet tends to have bigger fractionation. At the late stage when the jet becomes circular, the correlation function tends to approach 0.5 and maintain.

We now reveal the underlying mechanism of axis-switching as follows. Through close inspection of the secondary velocity field and vorticity on the transverse planes just before the axis-switching occurs, we are able to identify specific patterns for 45° and 90° axis-switchings, shown in Figs. 5 and 6 respectively, which are considered as the triggers for the axis-switchings. In Fig. 5, it can be seen that the velocity at the four corners of jet profile is uniformly toward the center while the flow is expanding outward at the four sides. Meanwhile, corresponding vorticity fields indicate that 45° axis-switching

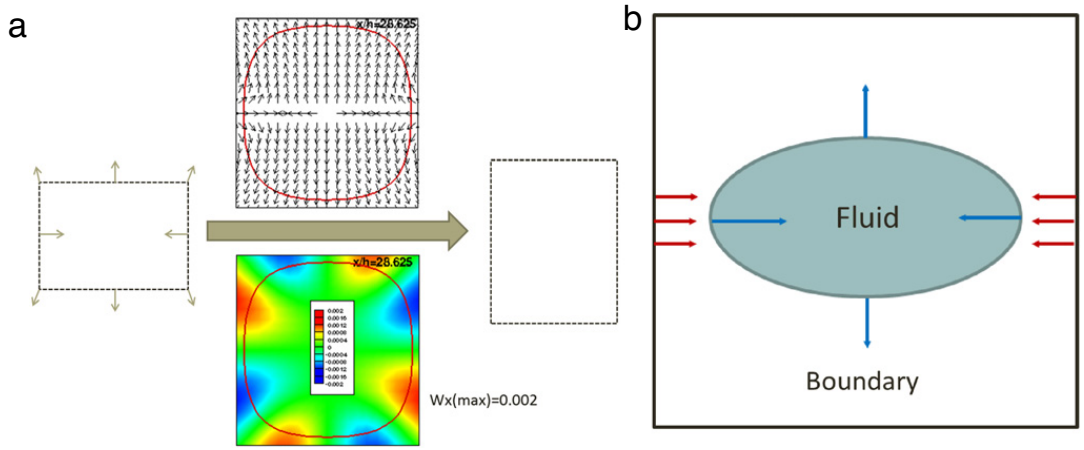

Fig. 6. Driven mechanism of flow and vorticity patterns for 90° axis-switching. Rectangular jet ($AR = 1.5$).

follows the occurrence of vortex pairs at the corners, which contribute a centripetal momentum and thus result in 45° axis-switching afterward. This mechanism applies to 45° axis-switching in both square and rectangular jets. The difference between 45° axis-switching in square (Fig. 5(a)) and rectangular jet (Fig. 5(b)) is that in the latter the pair of vorticity along spanwise is stronger than that along lateral while both pairs are equally strong in the former. Similar approach is applied to shed some light on 90° axis-switching in rectangular jets. The 90° axis-switching is driven by a different pattern as shown in Fig. 6. There is strong inflow stream along spanwise and outflow stream along lateral, driving the jet to elongate in the lateral direction. The boundary effect is profound for 90° axis-switching. When the jet develops, the major direction approaches the boundary first and is squeezed by the boundary, leading the flows changes from the major to minor direction, to 90° axis-switching. The vorticity point view is no more applicable since its magnitude has become very small (0.002) in Fig. 6(a) compared to 0.03 in Fig. 5(b) to exert an influence on bringing about 90° axis-switching.

4. Conclusion

Through direct numerical simulation using the lattice Boltzmann method, we systematically studied axis-switching phenomena in five low aspect-ratio rectangular jets. Although the axis-switching in elliptic jet was extensively studied in the past, axis-switching behavior in rectangular jets is more complicated due to the fact that rectangular jets combine the variable aspect-ratio feature of elliptic jets with the corner vortex feature of square jets. The underlying fluid dynamical mechanism is far from clear. In this work, we focus on the correlation between downstream velocity and secondary flow. The development of the half-width streamwise velocity contour (HWSVC) lines clearly exhibits two concessive axis-switchings when the jet is propagating, indicating richer mixing features than square or elliptic jets. The 45° axis-switching occurs shortly after the jet enters the characteristic decay (CD) region while 90° appears when the jet is about to exit from the CD region toward the axisymmetric decay region. It is found that the location of 45° axis-switching is independent of the jet *AR* but the shape of the 45° axis-switching varies with different *AR*, implying that the 45° axis-switching is contributed by both corner feature and elliptic feature. The 90° axis-switching seems to have a different story. As the jet develops, it spreads through the mixing and entrainment with the surroundings. When the flow in the major axis approaches the boundary, the entrainment in the major axis is weakened while the mixing along the minor axis becomes competitive to the major axis. As the jet further develops, the flow along minor axis exceeds that along the major axis, which is how the 90° axis-switching occurs. In our study, we synthesized two specific patterns to reveal the underlying dynamics from the secondary velocity field and vorticity contour to unveil the mechanism of the 45° and 90° axis-switchings.

The mechanisms of 45° and 90° axis-switching in laminar jets suggest the independency of axis-switching behavior to the Re number, whereas the downstream location where axis-switching occurs will vary for different Re numbers. Based on the current work plus a turbulent inlet velocity profile we have developed very recently, we plan to revisit the axis-switching in turbulent rectangular jets focusing on the Re number effects on axis-switching development in the next step.

Acknowledgments

This work is supported by Research Support Funds Grant (RSFG) from the Office of the Vice Chancellor for Research (OVCR), Indiana University–Purdue University Indianapolis and the National Nature Science Foundation of China under Grant No. 11072229.

References

[1] E.J. Gutmark, F.F. Grinstein, Flow control with noncircular jets, Annu. Rev. Fluid Mech. 31 (1999) 239.
[2] H.S. Husain, A.K.M.F. Hussain, Controlled excitation of elliptic jets, Phys. Fluids 26 (1983) 2763.

[3] C.M. Ho, E. Gutmark, Vortex induction and mass entrainment in a small-aspect-ratio elliptic jet, J. Fluid Mech. 179 (1987) 383.
[4] E. Gutmark, K.C. Schadow, Flow characteristics of orifice and tapered jets, Phys. Fluids 30 (1987) 3448–3454.
[5] K. Toyoda, F. Hussain, Vortical structures of noncircular jets, in: Proceedings of the Fourth Asian Congress of Fluid Mechanics, Hong Kong, 21–25 August 1989, pp. A117–A127.
[6] F. Hussain, H.S. Husain, Elliptic jets. Part 1. Characteristics of unexcited and excited jets, J. Fluid Mech. 208 (1989) 257.
[7] S.B. Verma, E. Rathakrishnan, Influence of aspect-ratio on the mixing and acoustic characteristics of plain and modified elliptic slot jets, Aerosol Sci. Technol. 7 (2003) 451–464.
[8] J.-H. Yoon, S.-J. Lee, Investigation of the near-field structure of an elliptic jet using stereoscopic particle image velocimetry, Meas. Sci. Technol. 14 (2003) 2034–2046.
[9] W. Zhao, K. Kumar, A.S. Mujumdar, Flow and heat transfer characteristics of confined noncircular turbulent impinging jets, Drying Technol. 22 (9) (2004) 2027–2049.
[10] V.D. Kasyap, D. Sivakumar, B.N. Raghunandan, Flow and breakup characteristics of elliptical liquid jets, Int. J. Multiph. Flow 35 (2009) 8–19.
[11] D.H. Kwon, S.J. Lee, Axis-switching of non-axisymmetric microdroplet ejected from inkjet with an elliptical nozzle, Phys. Fluids 23 (2011) 051703.
[12] G. Amini, A. Dolatabadi, Axis-switching and breakup of low-speed elliptic liquid jets, Int. J. Multiph. Flow 42 (2012) 96–103.
[13] G.F. Marsters, J. Fotheringham, The influence of aspect ratio on incompressible turbulent flows from rectangular slots, Aeronaut. Q. 31 (1980) 285.
[14] G.F. Marsters, Spanwise velocity distributions in jets from rectangular slots, AIAA J. 19 (1981) 148.
[15] Y. Tsuchiya, C. Horikoshi, T. Sato, On the spread of rectangular jets, Exp. Fluids 4 (1986) 197.
[16] W.R. Quinn, Development of a large-aspect-ratio rectangular turbulent free jet, AIAA J. 32 (1994) 547.
[17] T.S. Chyczewski, L.N. Long, P.J. Morris, Numerical study of nozzle exit condition effects on jet development, AIAA J. 36 (6) (1998) 986–993.
[18] K.H. Luo, Axis switching in turbulent buoyant diffusion flames, in: Proceedings of the Combustion Institute, Vol. 30, 2005, pp. 603–610.
[19] H. Yu, S.S. Girimaji, Near-field turbulent simulations of rectangular jets using lattice Boltzmann method, Phys. Fluids 17 (2011) 125106.
[20] H. Yu, S.S. Girimaji, Lattice Boltzmann equation simulation of rectangular jet ($AR = 1.5$) instability and axis-switching, Physica A 362 (2006) 151–157.
[21] H. Yu, S.S. Girimaji, Study of axis-switching and stability of laminar rectangular jets using lattice Boltzmann method, Int. J. Comput. Math. Appl. 55 (2008) 1611–1619.
[22] E.J. Gutmark, K.C. Schadow, T.P. Parr, D.M. Hanson-Parr, K.J. Wilson, Noncircular jets in combustion systems, Exp. Fluids 7 (1989) 248.
[23] M. El Hassan, A. Meslem, Time-resolved stereoscopic PIV investigation of the entrainment in the near field of circular and daisy-shaped orifice jets, Phys. Fluids 22 (2010) 035107.
[24] F. Krebs, F. Silva, D. Sciamarella, G. Artana, A three-dimensional study of the glottal jet, Exp. Fluids 52 (2012) 1133–1147.
[25] S. Chen, G.D. Doolen, Lattice Boltzmann method for fluid flows, Annu. Rev. Fluid Mech. 30 (1998) 329.
[26] C.K. Aidun, J.R. Clausen, Lattice–Boltzmann method for complex flows, Annu. Rev. Fluid Mech. 42 (2010) 439–472.
[27] X. He, L.-S. Luo, Theory of the lattice Boltzmann method: from the Boltzmann equation to the lattice Boltzmann equation, Phys. Rev. E 56 (1997) 6811–6817.
[28] H. Wang, S. Menon, Fuel–air mixing enhancement by synthetic microjets, AIAA J. 39 (12) (2001) 2308–2319.
[29] T. Mautner, Application of the synthetic jet concept to low Reynolds number biosensor microfluidic flows for enhanced mixing: a numerical study using the lattice Boltzmann method, Biosens. Bioelectron. 19 (2004) 1409–1419.
[30] X. He, L.-S. Luo, Lattice Boltzmann model for the incompressible Navier–Stokes equation, J. Comput. Phys. 88 (1997) 927.
[31] L.-S. Luo, Theory of the lattice Boltzmann method: lattice Boltzmann models for nonideal gases, Phys. Rev. E 62 (2000) 4982–4996.
[32] P.M. Sforza, M.H. Steiger, N. Trentacoste, Studies on three-dimensional viscous jets, AIAA J. 4 (1966) 800.
[33] P.M. Sforza, A quasi-axisymmetric approximation for turbulent three-dimensional jets and wakes, AIAA J. 7 (1969) 1380.
[34] N. Trentacoste, P.M. Sforza, Further experimental results for three-dimensional free jets, AIAA J. 5 (1967) 885.
[35] A.A. Sfeir, The velocity and temperature fields of rectangular jets, Int. J. Heat Mass Transfer 19 (1976) 1289.
[36] A.A. Sfeir, Investigation of three-dimensional turbulent rectangular jets, AIAA J. 17 (1979) 1055.